

Role of 'O' Substitution in Expanded Porphyrins on Uranyl Complexation: Orbital and density based analyses

Saparya Chattaraj,^{†,‡} Arunasis Bhattacharyya,^{*,¶,‡} and Biswajit Sadhu^{*,†}

[†]*Health Physics Division, Health Safety and Environment Group, Bhabha Atomic Research
Center, Mumbai – 400 085, India*

[‡]*Homi Bhabha National Institute, Anushaktinagar, Mumbai-400 094, India*

[¶]*Radiochemistry Division, Radiochemistry and Isotope Group, Bhabha Atomic Research
Center, Mumbai – 400 085, India*

E-mail: arun12@barc.gov.in; bsadhu@barc.gov.in, biswajit.chem001@gmail.com

Abstract

The need for efficient macrocyclic ligands that can sequester U(VI) has gained immense importance due to the increased applications of U(VI) in various sectors, including but not limited to nuclear energy. Structural attributes such as number and type of donor centers (“hard” and “soft”) of ligands are essentially the key components for providing the adequate bonding scenario for uranyl. Beside hard or soft-donor-based binding cavity, the mixed-donor ligands are also finding popularity for achieving optimized performances. However, many aspects are still unknown about how and at what extent the ratio of hard-to-soft donor centers tune the bonding attributes with uranyl. Moreover, a consensus is yet to be reached on the nature and role of underlying covalent interaction between U and donors upon complexation, particularly in the mixed-donor ligand environment. In this work, using relativistic density functional theory (DFT), we attempted to address these important issues by systematically investigating the impact on the bonding characteristics of uranyl ion and an expanded porphyrin, viz. sapphyrin with increasing number of 'O' substitution at the cavity. Our results suggest that in the O-substituted sapphyrin variants, UO_2^{2+} prefers to bind N over O donor sites, and decrease in N donor sites at the cavity prompts UO_2^{2+} to have better interaction with the rest of N donor centers. Extended transition state (ETS) with natural orbital for chemical valences (NOCV) analysis shows that at equatorial plane N acts as better σ donor to uranyl than O donor. Molecular orbital (MO) and density of states (DOS) analysis shows favorable bonding-interaction between U(d) and donor's p orbitals, the participation of U(f)-orbitals in bonding are of low-extent but non-negligible. Energy decomposition analysis (EDA), natural population analysis (NPA) along with thermodynamic analyses confirms the dominance of electrostatic interaction on the thermodynamic stability of the complexes. However, the U-N/O bonds at the equatorial plane do carry appreciable amount of covalent character. Analysis of quantum theory of atoms in molecules (QTAIM) descriptors in conjugation with MO analysis and overlap integral calculations confirms its nature as near-degeneracy driven type. Statistics of mixed-orbitals and overlap integral fur-

ther suggest that the O donor does not act as adequate replacement of N for uranyl binding despite having more number of mixed MOs due to the variation in the amplitude of overlap.

1. Introduction

The coordination chemistry of uranium (U) has been a pivotal research field that excites many branches of science and engineering communities. Apart from being an indispensable resource for nuclear energy,¹ the photophysical properties of uranium complexes^{2,3} have enhanced the importance of selective extraction of uranium from different matrices (e.g. aqueous waste). This has been central to the nuclear industry involving sectors such as mining of uranium, fabrication of nuclear fuel and reprocessing of the burnt fuel,⁴ and also found potent applications in environmental remediation.^{5,6} Amongst the several oxidation states of uranium, U(VI) is ubiquitously available (as UO_2^{2+}) in the radioactive wastewater, ocean water and soil due to the higher solubility of UO_2^{2+} . And, therefore the hunt for task-specific ligands that selectively sequester UO_2^{2+} have become an integral part of this field.^{7,8}

In the context of nuclear waste management, the choice of such ligands depend on two important criteria: A) the ligand should possess unique properties to selectively bind the actinide metal of interest with high affinity, and B) the secondary nuclear waste generated from the extraction process should be less toxic and incinerable.⁹ While the characteristics of donor centers, the cavity size and the backbone assisted conformational rigidity/flexibility (*albeit* at balanced proportion) within the ligand mainly decides its sequestering ability (i.e. fulfills criterion A), the second criterion is largely satisfied if the composition of the ligand has carbon (C), hydrogen (H), oxygen (O) and nitrogen (N) (i.e. follows CHON principle).⁹ In this regard, macrocycles such as crown ethers,^{10,11} calixarenes,¹² cucurbiturils,¹³ pyrrole-based expanded porphyrins¹⁴⁻¹⁶ has gained popularity as promising candidates.

Experimentally, it has been perceived that the modulation of cavity size by expanding the porphyrin ring can make it accessible for complexation with f-block elements.^{14,15} Recent reports on synthesis of series of An(IV) complexes with a class of expanded porphyrins has made a strong case on its applicability in actinide extraction. While these ligands contain soft N as the donor center for such task, ligands such as salens,¹⁷ pyrrophen utilizes both

soft N and hard O as the donor atoms to bind hard uranyl cation.¹⁸ This has immense implications in the presence of interfering cations. Following Hard-Soft-Acid-Base (HSAB) concept, it may be advisable to choose macrocyclic ligands with hard oxygen donor center for cation like U(VI), however, the extensive presence of lanthanides and other alkali metals within the nuclear waste often throws competition toward the efficiency of actinide extraction. Therefore, significant studies¹⁹⁻²¹ have been devoted on exploring how other alternative donor center such as ‘N’, ‘S’ or mixed-donor center (N,O) based ligands perform in chelation. Undoubtedly, availability of sophisticated quantum-mechanical techniques such as density functional theory (DFT) and advancement of tools that utilizes the orbital and density-based information have paved the way for understanding the actinide complexation with macrocycles in depth.^{22,23} Theoretical investigations on the uranyl complexes with variants of hexaphyrin ligands indicated that the change in size and shape of ligand’s cavity modulates the ionic/covalent character of metal-ligand bonds and subsequently alters the binding affinities.²⁴

Further, recent computational study²¹ led by some of us suggested that the change in donor center may tune the selectivity for specific actinide metals but could also potentially impact the thermodynamics of complexation. The perturbation of electronic structures with different set of donor centers often serve as an important attribute behind this, and the interaction of metal’s 5f and 6d along with relevant s and p orbitals of donors plays its part on the involved energetics.²⁵ Therefore, optimization on the number of hard and soft donors within the ligand core is an important factor on achieving a delicate balance between selectivity and binding affinity, and are central to the design principle for these ligands. However, there remains scarcity of knowledge on how systematic change of donor type and their ratio in mixed-donor environment impact the overall structure of complexes and the binding ability of ligands, and how that can be correlated with the subsequent alteration in the metal bonding properties.

Here we attempt to investigate these aforementioned issues using state-of-the-art rela-

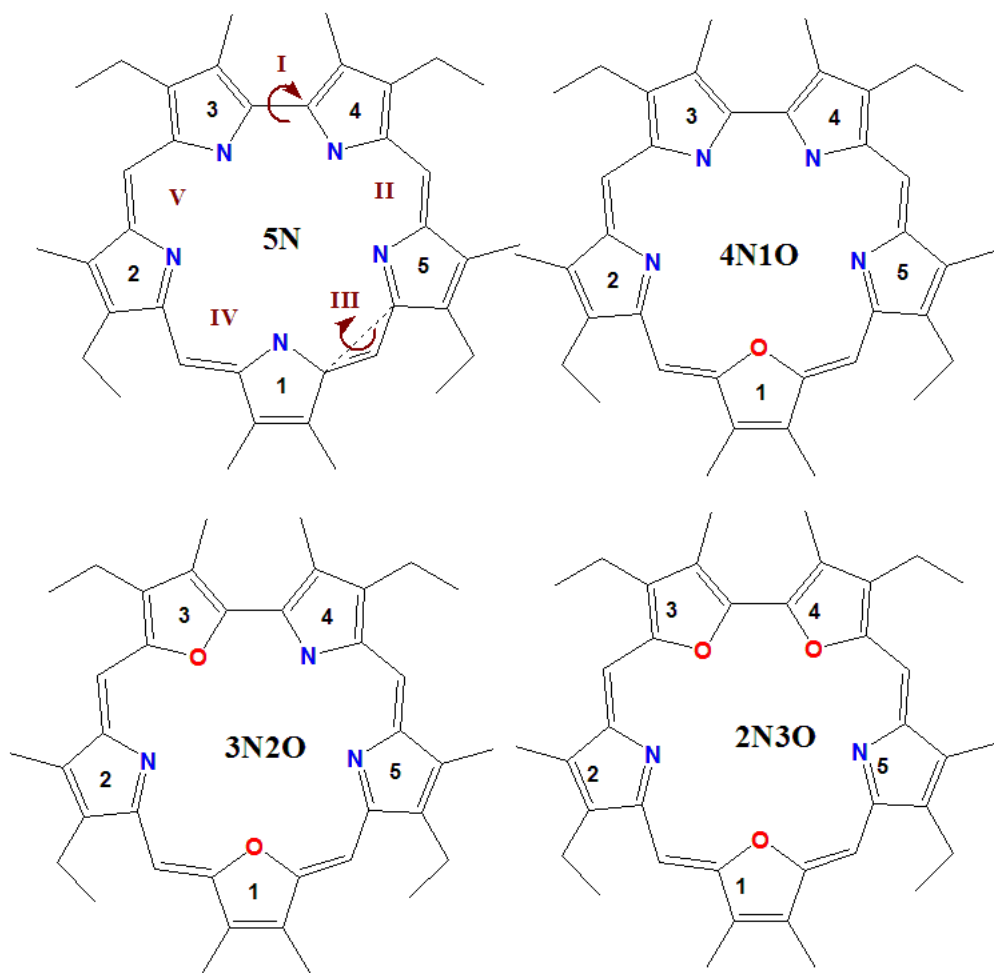


Figure 1: Schematic structures of sapphyrin, and oxasapphyrin analogues with varying N:O ratio. The name of the ligand indicate the number and type of donor center (e.g. ‘4N1O’ indicates that the corresponding ligand has four nitrogens and one oxygen donor atom.).N and O donor centers are shown in blue and red color, respectively. The two types of dihedral angles and associated indices are shown in brown color.

tivistic density functional theory (DFT) combining both orbital- and density-based analyses. We focus on the uranyl binding, and the architecture of oxasapphyrin are chosen as the design basis for complexation (cf. Fig 1). The choice of ligand can be justified because the cavity of oxasapphyrin provides penta-coordinated atmosphere with adequate cavity size (5.5 Å) to the uranyl ion as evident from the corresponding crystal structure of the uranyl-bound oxasapphyrin complex.²⁶ Further, the backbone of ligand can be expected to provide a greater extent of conformational rigidity to the ligand core, which is somewhat beneficial for comparing the bonding of uranyl cation with different ligand variants with different N:O ratio. We analyze the effect of donor center on complexation by considering three O-substituted sapphyrin variants that differs from each other with respect to the N:O ratio at the ligand core (cf. Fig 1). We primarily focus on understanding how and at what extent the varying ratio of N and O donor within the cavity alter the bonding attributes of uranyl ion and change the characteristics of metal-ligand bond at the equatorial plane. Applying a range of well-established methods such as quantum theory of atom in molecules (QTAIM), molecular orbital (MO) theory and energy decomposition analysis (EDA) with extended transition state-natural orbital chemical valence (ETS-NOCV) and density of states (DOS), we scrutinize the perturbation of ionic and covalent character of U-N and U-O bonds. Further, we attempt to assess the possible influence of altered bonding features over the thermodynamics of complexation.

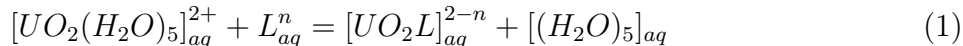
2. Computational and Analysis Methods

Here, we have considered sapphyrin as well as three analogues of oxasapphyrin ligand that contains different ratio of N and O donor centers. For better understanding, we named the ligands(Lⁿ; n=charge) based on the number and type of donor atoms: **5N**, **4N1O**, **3N2O** and **2N3O**. For instance, ‘4N1O’ indicates that the corresponding ligand has four N and one O donor atom. The initial structural coordinates for geometry optimization of the

uranyl-oxasapphyrin complex ($\text{UO}_2\cdot 4\text{N1O}$) were taken from the reported crystal structure by Sessler et al.²⁶ Structures of other ligands were custom-made by altering the donor centers. Notably, the feasibility of synthesizing such furan-pyrrole macrocycles following sapphyrin template has been demonstrated few-decades back by Broadhurst et al.²⁷ Owing to the high basicity at NH group of ligands, one can anticipate them to get deprotonated first in order to effectively bind the electron-dearth uranyl center. Keeping this in mind, we considered deprotonated form of the ligands as the primary reactant for the complexation. Among all the ligand variants, the sapphyrin (*i.e.* 5N) unit contains five N centers, and therefore it provides a pure environment that is devoid of any effect of O donor. Whereas, increasing number of O donor with subsequent decrease in N donors progressively enhances the role of O donor at the cavity as we approach from 4N1O to 3N2O to 2N3O.

Gas phase optimizations of all these structures were performed with tight energy convergence criteria ($10^{-8} E_h$) using the pure-GGA BP86 functional^{28,29} with def2-TZVP basis set³⁰ for all the elements except uranium, where def-TZVPP sets³¹ were used for the description of the valence electrons. During the optimizations, relativistic small-core effective core potential^{32,33} (SC-ECP) was used to model the core electrons of uranium. The confirmation that the optimized structures attained the potential energy minima was obtained by the absence of imaginary frequencies through analytical frequency calculations with the *AOFORCE* module of TURBOMOLE v7.2.³⁴ Thermodynamic quantities were evaluated with the *FREEH* module applying the default scaling factor (0.9914) at temperature (298.15 K). Single-point calculations on the optimized structures were performed at B3LYP^{35,36}/def2-TZVP level with zeroth-order regular approximation³⁷ (ZORA) using ORCA 3.0.3.³⁸ For both optimization and energy minimization, the Resolution of Identity (RI) (for optimization) and RIJCOSX³⁹ (for single points) approximations were employed in conjugation with the corresponding auxiliary basis sets to achieve optimum computation speed without losing much accuracy. The effect of implicit water solvation was accounted using the conductor-like polarizable continuum model⁴⁰ (CPCM) ($\epsilon=80.4$, $\eta=1.33$), as implemented in ORCA

3.0.3. For the explicit solvation effects at the primary solvation shell of uranyl cation, we have used penta-hydrated uranyl for the binding free energy calculations (ΔG_{bind} , equation 1). Note that, previous experimental and theoretical studies suggested five water molecules can remain directly coordinated with the uranyl center to complete its first coordination shell thus justifies the choice of hydration model of uranium.^{41,42} To be confident about the obtained trend in ΔG_{bind} , an additional set of calculation were performed using two other density functionals (BP86 and B2PLYP⁴³).



To understand the extent of participation of metal and ligand orbitals into the complex molecular orbitals, we performed molecular orbital (MO) analysis using ORCA-generated Löwdin orbital compositions. In addition, for deciphering the bonding/antibonding character of the orbital interactions, we studied the overlap population of density of state (OPDOS) for U(p,d,f)-O/N interactions. Further, in order to scrutinize the energetic contributions associated with the binding of uranyl, Kitaura and Morokuma’s energy decomposition analysis⁴⁴ (EDA) was employed on the optimized structures at the B3LYP/TZ2P⁴⁵/ZORA level using ADF 2017.⁴⁶ Within the framework of EDA, the bonding energy (ΔE_{bond}) of the complex is decomposed into following interaction terms: stabilizing electrostatic interaction (ΔE_{ion}), orbital interaction (ΔE_{orb}) arising from the orbital relaxation of fragment molecular orbitals (FMOs), and repulsive Pauli exchange interaction from the fragments of same-spin (ΔE_{Pauli}). Further, ΔE_{orb} , which also accounts for the charge-transfer and polarization energy, was decomposed applying Extended Transition State (ETS) theory in combination with the Natural Orbital for Chemical Valence (NOCV) method⁴⁷ to elucidate the various deformation-density channels of σ/π /back-donation between the chosen fragments (*i.e.* UO_2^{2+} and L^n , n=charge of the ligand).

For partial charge analysis, we employed Natural Population Analysis (NPA), which arguably has been shown to work better in describing the actinide-ligand bond with minimal

basis-set dependency.^{48,49} Furthermore, to understand the variation of ionic and covalent character in uranyl-ligand bonding, we evaluated the trends in various QTAIM descriptors, namely charge density(ρ), Laplacian of the electron density ($\nabla^2\rho$), the kinetic energy density ($H(r)$), the ellipticity(ϵ) and the ratio of the potential energy to the Lagrangian kinetic energy ratio ($|V(r)/G(r)|$). Notably, Bader’s QTAIM analyze the bond by partitioning molecular electron density ($\rho(r)$) region at zero flux surface and explains bond formation by a (3,-1) bond critical point (BCP). The properties at the BCP contain nontrivial information related to the electron density sharing and provide quantitative basis to comment on the nature of covalency (overlap-based or near-degeneracy driven).^{21,50–53} Within QTAIM framework,^{54,55} $\rho(r) < 0.2 \text{ e/Bohr}^3$, positive $H(r)$ along with positive $\nabla^2\rho$ at BCP suggest closed-shell interaction, whereas $\rho(r) > 0.2 \text{ e/Bohr}^3$ with negative $\nabla^2\rho$ indicates covalent interaction between two coordinating atoms. A negative $H(r)$ along with a positive $\nabla^2\rho$ indicates an intermediate type interaction like polar covalent.^{54,55} For more details on the QTAIM method, we refer the readers to the following original work.^{54–56}

3. Results and discussion

3.1. Structural perturbation in bare ligands with varying N:O ratio:

As an important and rational step, we first analyze the structural changes within the ligands upon O donor substitutions. As mentioned earlier, sapphyrins are known to have strong basic properties⁵⁷ so the deprotonation of the pyrrole NH group (of ligand containing NH) appears to be a prerequisite step before complexation with uranyl ion. It is important to mention here that 5N ligand-variant in Figure 1 contains three such NH groups (in pyrrole ring 1,3,4) in its protonated form, which makes the N of pyrrole ring 1,3,4 more basic as compared to other N donor (i.e. in pyrrole ring number 2 and 5). Keeping this in mind, throughout the paper, we provide separate results for two of these classes of N donor (except in ‘2N3O’ where only one class of N donors exist). This approach also seems logical considering the

fact that the substitution with O donor is performed at the NH site. This could trigger an enhanced localized change in the electron density distribution at the replaced site. In fact, later in this article, we would show that these two classes of N donor centers indeed have some variations which categorically separate them from each other.

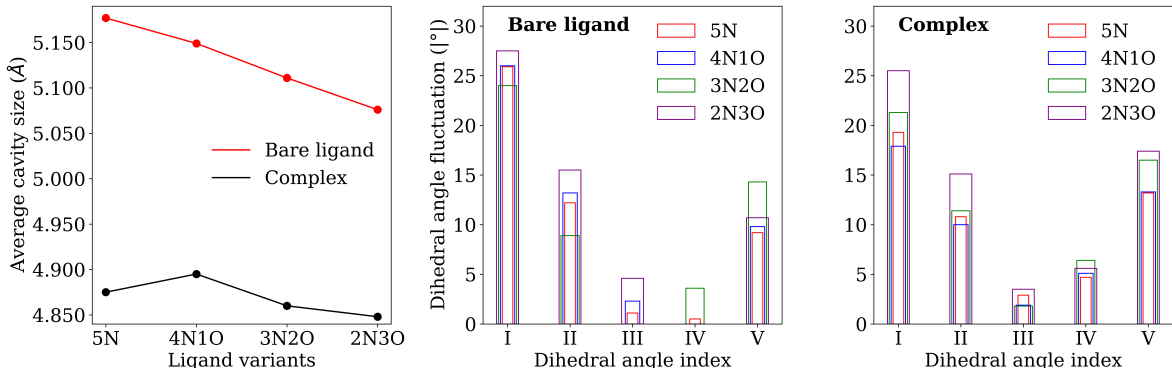


Figure 2: Change in cavity size and dihedral angle fluctuation within the bare ligands and complexes.

We scrutinize the structural perturbation within the ligand by analyzing two geometrical aspects, namely cavity size and dihedral angle distribution (cf. Figure 2). The average cavity size (in Å) is determined by averaging the sum of distances between alternate donor centers. We noted that increasing O donor centers at the ligand core prompts a steady decrease in the average cavity size values. In order to comment on how it perturbs the coplanarity of the ligand core, we relied on the distribution of five dihedral angles (‘I’-‘V’) that are formed between the adjacent pyrrole rings involving their donor center (cf. figure 1). We found that among all the dihedral angles, distortion in absolute sense is maximum for ‘I’ (*i.e.* for the plane connecting ‘3’ and ‘4’ pyrrole ring) irrespective of the donor center composition of ligand core. This is in accord with the experimental observation⁵⁸ and can be attributed to the lack of meso carbon atom between ring ‘3’ and ‘4’. As a consequence, the nearest two torsions (*i.e.* ‘II’ and ‘V’) of ‘I’ get affected more as compared to ‘III’ and ‘IV’. Importantly, it is evident from figure 2 that change in the ratio of N:O does not substantially ($< 4^\circ$ change in coplanarity) perturb the coplanarity of the ligand core but rather helps in tuning

the cavity size, which indeed provides confidence about the conformational stability of the ligands.

3.2. Structural changes in uranyl complexes with varying N:O ratio of the ligand:

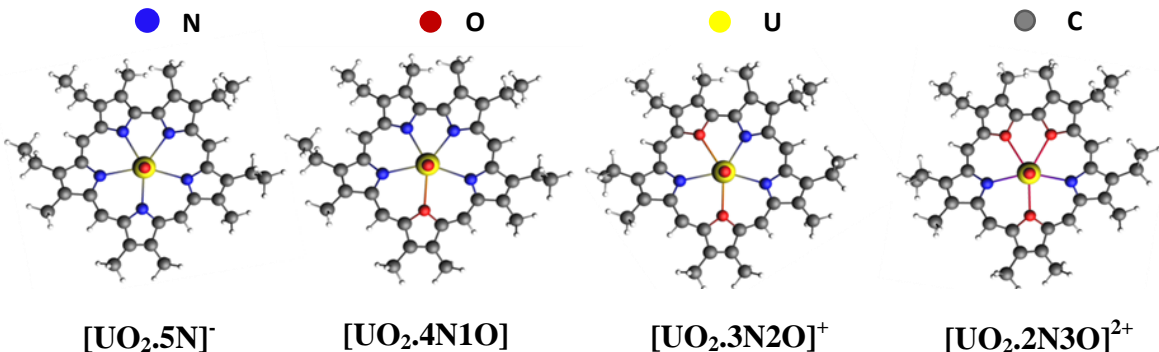


Figure 3: Optimized structures of the UO₂-ligand complexes. (Color code: U: yellow, O: red, N: blue, C: deep grey, H: light grey)

Table 1: Optimized structural parameters involving the central uranium and donor atoms (X = N,O).

Complex	U-X _{eq} bond length (Å) ^{a,b}			U-N _{2,5}	U-O _{ax} bond length (Å)	U _{ax} -U-O _{ax} bond angle (°)
	U-N	U-X _{1,3,4}	U-O			
[UO ₂ .5N] ⁻	2.545, 2.545, 2.548 (2.546)	-	-	2.606, 2.609 (2.607)	1.795, 1.796 (1.795)	178.3
[UO ₂ .4N1O]	2.472, 2.475 (2.473) [2.450, 2.470 (2.460)]	2.762 [2.791]	2.762 [2.791]	2.585, 2.591 (2.588) [2.582, 2.586 (2.584)]	1.788, 1.788 (1.788) [1.762, 1.767 (1.764)]	174.0 [176.3]
[UO ₂ .3N2O] ⁺	2.459	2.651, 2.666 (2.658)	2.651, 2.666 (2.658)	2.490, 2.552 (2.521)	1.781, 1.782 (1.782)	176.7
[UO ₂ .2N3O] ²⁺	-	2.569, 2.649, 2.652 (2.623)	2.569, 2.649, 2.652 (2.623)	2.465, 2.467 (2.466)	1.775, 1.775 (1.775)	178.6
[UO ₂ .5H ₂ O] ²⁺	-	2.464, 2.471, 2.472, 2.490, 2.490 (2.477)	2.464, 2.471, 2.472, 2.490, 2.490 (2.477)	-	1.765, 1.765 (1.765)	176.6

^aValues in parenthesis correspond to the average values, ^bValues within the square bracket correspond to the crystal structure²⁶ of [UO₂.4N1O]

Optimized structures of uranyl complexes are presented in Figure 3. The reported crystal structure of [UO₂.4N1O] complex confirms that the arrangement of donor centers and the

cavity size of 4N1O ligand are adequate for uranyl chelation. Our optimized structure of [UO₂.4N1O] is noted to be in excellent correlation with the crystal structure (RMSD: 0.835 Å). For instance, the average U-N and U-O_{eq} bond distances are found within 0.03 Å when compared with the crystal structure.²⁶ For all the ligands with N donors at pyrrole ring 1, 3 and 4, U-N_{1,3,4} bond length is always found to be smaller than U-N_{2,5} bond, indicating much stronger interaction of U(VI) with the former N donors. Further, U-N_{1,3,4} bond length is observed to decrease as one traverses from 5N to 4N1O to 3N2O ligand. Similar trend is also followed by the U-N_{2,5} and U-O_{eq} bond lengths (cf. Table 1). These observations nicely corroborate the overall decrease in cavity size of ligands (with increasing O donor centers) after complexation, which allows U to achieve adequate interactions (shorter bond distances) with ligand donors (cf. Figure 2). A quick comparison of U-O_{water} bond in [UO₂(H₂O)₅]²⁺ with the U-O_{eq} bond lengths (of ligand variants) suggest significantly shorter bond length for the former. This possibly suggests that the constrained environment or the conformational rigidity of the investigated expanded porphyrins has somewhat restrictive influence over the U-O_{eq} bonding strength.

3.3. Electronic structures of the complexes:

3.3.1. Partial charge analysis:

Table 2: Derived partial atomic charges (a.u.) of complexes and ligands using natural population analysis (NPA).

Complex	NPA charges					
	U	O _{ax}	O _{1,3,4}	N _{1,3,4}	N _{2,5}	Charge transfer to [UO ₂] ⁺² (LMCT)
[UO ₂ .5N] ⁻	1.840	-0.598	-	-0.509	-0.481	1.356
[UO ₂ .4N1O]	1.888	-0.579	-0.438	-0.513	-0.488	1.270
[UO ₂ .3N2O] ⁺	1.928	-0.563	-0.433	-0.503	-0.525	1.198
[UO ₂ .2N3O] ⁺²	1.976	-0.550	-0.441	-	-0.535	1.124

Charge transfer analysis on the optimized structures can provide critical insight over the

donor-acceptor relationship between the ligand and metal. It is important to note here that the overall charge of the ligand (fully deprotonated) becomes more positive as we traverse from 5N to 2N3O. Therefore, the partial charges obtained from NPA for uranium is found to be progressively more positive toward 2N3O (cf. Table 2). Further, the negative charge density (average) at the deprotonated N_{1,3,4} atoms is noted to be higher as compared to the N_{2,5} donor centers despite having shorter U-N_{1,3,4} bond length than U-N_{2,5} (Table 1). Between N and O donor atoms, the partial negative charges were found to be smaller on O atoms, which can be due to the difference in their electronegativity (*i.e.* “softness”). Our obtained result suggests a decreasing trend in ligand to metal charge transfer (LMCT) as we traverse from 5N to 2N3O ligand, which partly could be accredited to the decrease (*i.e.* more positive) in overall charge of complexes toward 2N3O. This has immediate impact over the negative charge density on the axial oxygen (O_{ax}) and U-O_{ax} bond distances. As the charge of the complexes become more positive (e.g. [UO₂.3N2O]⁺ and [UO₂.2N3O]²⁺), negative charge on O_{ax} flows toward U, which leads to shortening of U-O_{ax} bond length (Table 1) with lower share of the negative charge on O_{ax} atoms.

Table 3: Wiberg bond indices and delocalisation indices for complexes.

Complex	Wiberg Bond Indices				Delocalisation Indices			
	U-O _{ax}	U-O _{1,3,4}	U-N _{1,3,4}	U-N _{2,5}	U-O _{ax}	U- O _{1,3,4}	U- N _{1,3,4}	U- N _{2,5}
[UO ₂ .5N] ⁻	2.049	-	0.422	0.394	1.899	-	0.355	0.326
[UO ₂ .4N1O]	2.072	0.174	0.476	0.404	1.929	0.146	0.413	0.343
[UO ₂ .3N2O] ⁺	2.089	0.209	0.490	0.463	1.951	0.181	0.430	0.403
[UO ₂ .2N3O] ⁺²	2.104	0.222	-	0.523	1.972	0.202	-	0.465

We also looked into the delocalization indices (DIs)⁵⁹ and Wiberg bond indices (WBIs) (cf. Table 3) to confirm on the electron sharing between the donor and acceptor atoms. Indeed, these metrics indicated an increase in the bond-order for U-O_{ax} with increasing positive charge of the complex. The trends observed in both of these descriptors are in excellent agreement with each other. A comparative analysis between U-O_{eq} and U-N bonds suggests larger electron sharing with N donor center and possibly indicates higher covalent

character. Surprisingly, we noted an increase in U-N bond indices and shared electron population despite the fact that the overall charge of the complex becomes progressively positive toward 2N3O. This observation probably suggests that the sequential increase in the number of oxygen donor centers at the ligand’s core has significant influence over the U-N bond and somewhat contributes to enhance its associated covalent character. To investigate further on these aspects, we performed in-depth molecular orbital analysis on the complexes.

3.3.2. Molecular orbital analysis:

Scrutiny of natural electron configuration of uranium shows an increase in 5f electron population at the expense of 6d orbital as number of O donors increases at ligand’s cavity (Supporting information, Table S1), suggesting the possible perturbation in the participation of 5f and 6d orbitals into bonding. However, it can be somewhat deceptive to comment on the role of U orbitals with O donors at equatorial plane due to the dominant bonding involvement of O_{ax} atoms (with U). Nevertheless, the participation of s and p orbitals of donor centers are found to have larger population indicating their strong participation into bonding with U. To have more quantitative picture on this, we obtained count-statistics on the number of mixed-orbitals for all possible type of interactions among uranium (s,p,d,f) and donor-center (*i.e.* O_{eq}/N) based orbitals (s,p).

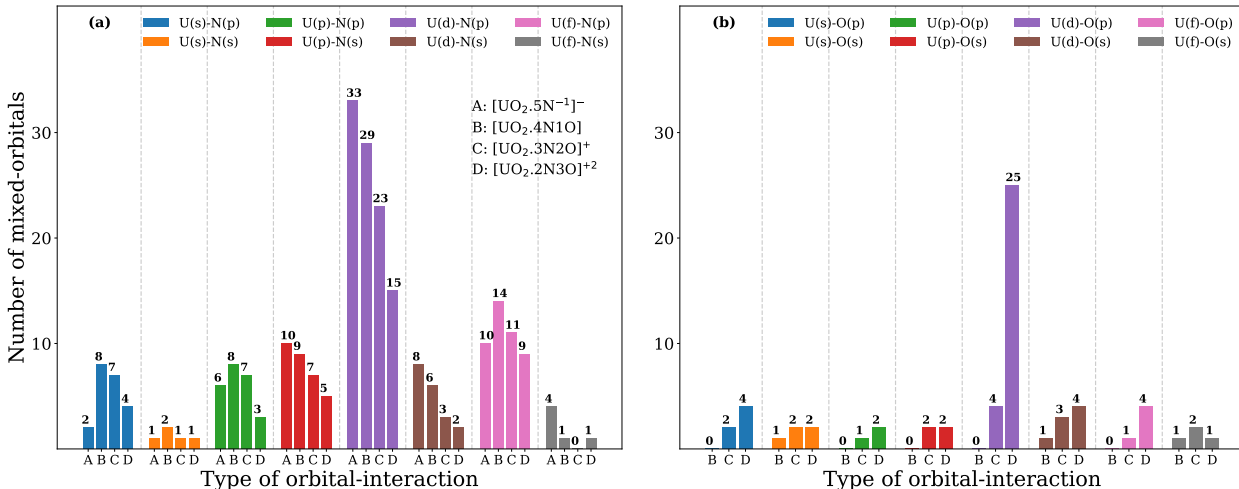


Figure 4: Count-statistics of mixed-orbitals based on involved metal and ligand orbital-type.

Here, we define only those orbitals as mixed-orbitals which have metal and donor-center(O_{eq}/N) contribution higher than 2% for the specific associated orbital type. For the computation, orbitals with energy < 5 eV is only considered. For U-N interaction, the obtained counts indicate that U(d)-N(p) interaction is the dominant among other possible interactions with maximum number of mixed-orbitals, followed by the U(f)-N(p), U(p)-N(s) interactions. Number of mixed-orbitals for U(s)-N(p), U(p)-N(p), U(d)-N(s) interactions are noted to be comparable, whereas U(s)-N(s) and U(f)-N(s) interaction have least contributions in the mixed molecular orbitals. Further, it is apparent from the trend that upon replacement of N donors the number of mixed-orbitals involving N(s,p) decrease progressively with subsequent increase in the U-O based mixed-orbitals. Such increase is particularly evident for U(d)-O(p) interaction. These results confirms that electron donation from O and N donors majorly occurs into the empty d orbitals of U.

We further analyzed up to what extent metal and donors (O_{eq}/N) contributes to the mixed-orbitals by plotting a bi-dimensional histogram (Figure 4) for all the complexes. For this analysis, we extracted those molecular orbitals which has higher than 2% metal character (with summed contribution of s, p, d and f) as well as 2% donor-center character (with summed contribution of s and p). The resulted plot suggests that irrespective of the complex type, majority of the mixed-orbitals are those which carries lower percentage ($< 20\%$) metal and donor center character. Interestingly, we found that with increasing O donor at the cavity leads to gradual increase to such instances.

Finally, we gauged into the U-based molecular orbital (MO) energy diagram to comment on its distribution with respect to the orbital energy (eV) (Figure 6 and Supporting information, Figure S1). It can be perceived from the plot that U(f)-based MOs above the highest occupied molecular orbital (HOMO) remain majorly localized with significant % of f-character. Whereas, some of the MOs with moderate f-character stays well below HOMO, suggesting U(f) orbitals do participate into bonding, *albeit*, in small extent. Another interesting observation is the successive stabilization of p, d and f-based low-lying occupied MOs

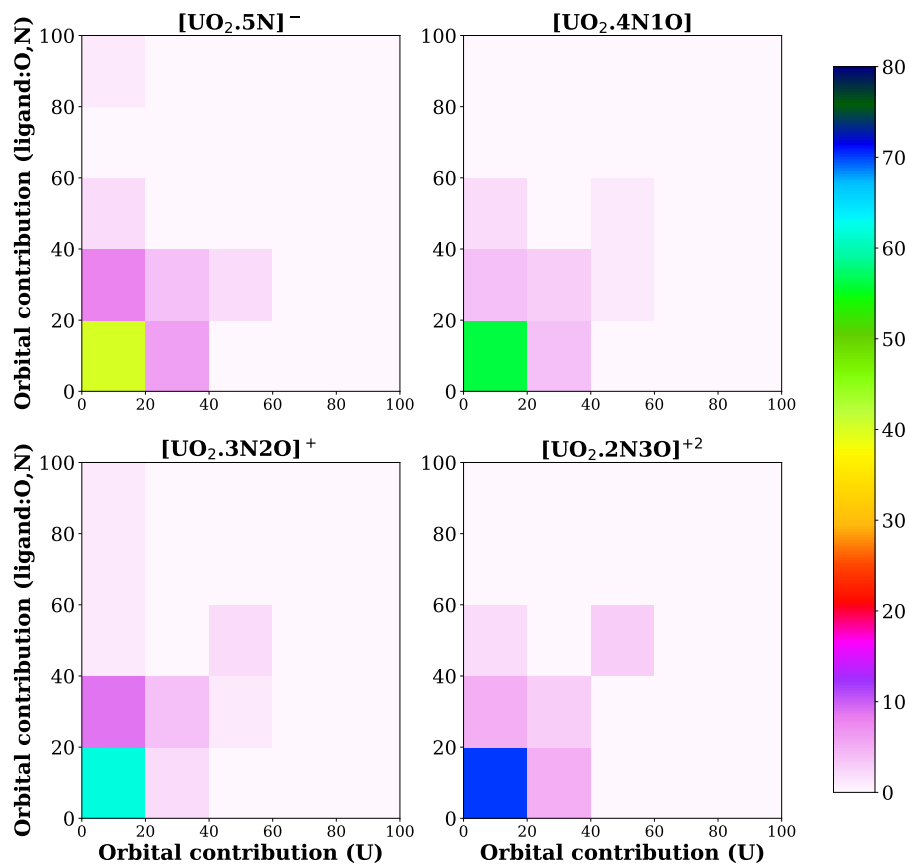


Figure 5: 2D-histogram quantifying instances of the mixed-orbitals comprising more than 2% metal as well as donor-center contribution. The color bar indicates the count associated with the bin and reflects the number of corresponding mixed-orbitals within the bin.

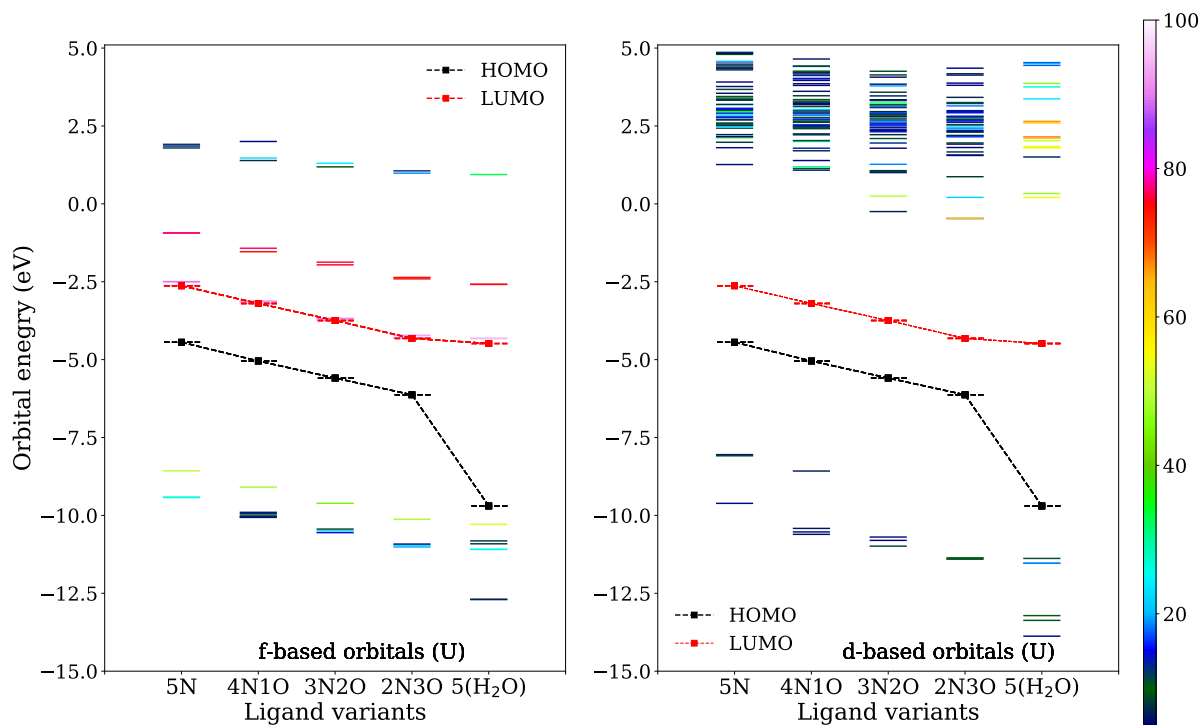


Figure 6: Molecular orbital energy diagram: Distribution of f- and d-based orbitals (> 10%) with respect to the orbital energy in metal–ligand complexes. The color of the orbital indicates % of specified metal-orbital character in that molecular orbital.

as we move towards ligands with more oxygen donor center. This stabilization can be linked to the difference in the distribution of s and p orbitals of O and N donor centers in bare ligands (supporting information, Figure S2). Close inspection on the distribution of s and p orbitals of donor centers indicates that s and p-based orbitals of N majorly lie close to HOMO while such orbitals of O are relatively low-lying in nature. More number of O donors and subsequently lower number of N donors within a ligand apparently reduce the energy of mixed bonding orbitals with U (p,d,f) occupied orbitals. Further, within the range (-5,+15 eV), majority of the U(s), U(p) and U(d)-based MOs are found to lie as virtual unoccupied orbitals with low to moderate contribution. The larger spread of diffused d-based MOs as compared to the f-based MOs nicely correlates with the greater participation of U(d)-orbitals into bonding (Figure 5). In order to have a qualitative understanding on ligands with five oxygen donor centers, we also looked into the MO energy diagram of $\text{UO}_2(\text{H}_2\text{O})_5^{2+}$ (Figure 6 and Supporting information, Figure S1). Evidently, with the increase in O donors, the distribution of U-based MOs somewhat converges to the case of $\text{UO}_2(\text{H}_2\text{O})_5^{2+}$. The large HOMO-LUMO gap of $\text{UO}_2(\text{H}_2\text{O})_5^{2+}$ as compared to the studied complexes may be accredited to the different composition of donor centers and conformational rigidity of ligands that possibly reduces the degree of freedom of ligand to inhibit relaxed metal-ligand bonding.

Further, to comment on the bonding/antibonding character of the complex MOs formed by the interaction of U(p,d,f) with donors, we analyzed the overlap population density of states (OPDOS) (Figure 7). The plots show in occupied MOs, f and d orbital of U participate in bonding interaction (*i.e.* stabilizing) with the donor center irrespective to the donor type, whereas interaction among U(p) orbitals and O/N is of antibonding type (*i.e.* destabilizing). Further scrutiny on the overlap population suggest that the intensity of such bonding interaction is significantly higher for U(d) as compared to U(f). Close inspection of OPDOS of donor center with respect to the bonding interaction reveals higher extent of bonding character for U(d,f)-N as compared to U(d,f)-O. It is not only indicative of higher covalent character for U-N bonds but also suggests that the replacement of N with O does

not compensate or makeup for the stabilizing bonding interaction.

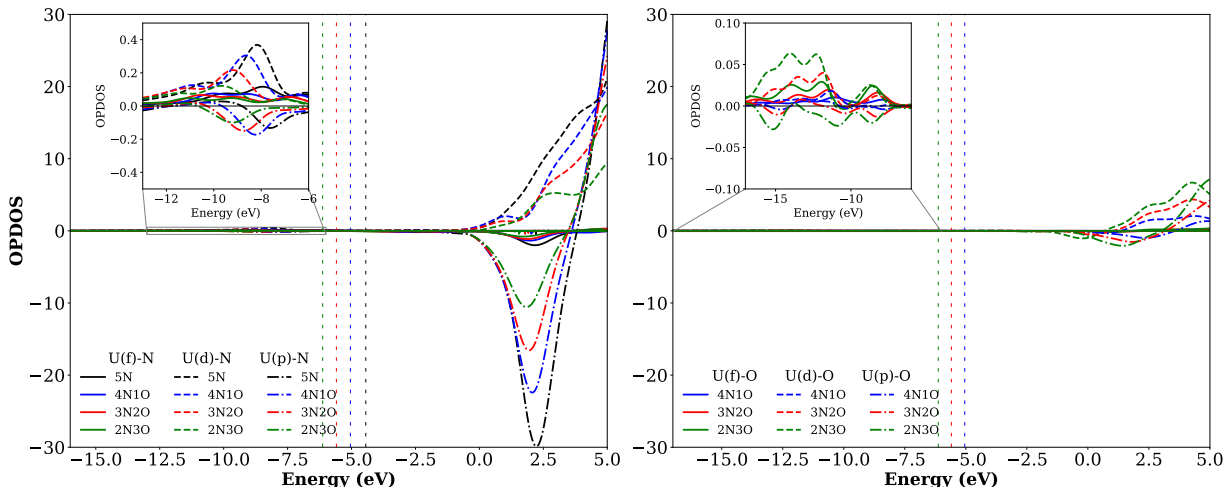


Figure 7: The overlap population density of states (OPDOS) diagram for all complexes. Left panel shows OPDOS plot for U(p,d,f) and N donor centers. Right panel shows OPDOS plot for U(p,d,f) and O donor centers at equatorial plane of U. The energy level correspond to HOMO of the complexes are shown using vertical dashed lines.

Effect of donor substitutions on orbital mixing and overlap integrals:

As mentioned in the preceding section, the increase in O donors led to increase of those mixed-orbitals which contains lower contribution of U and donors ($< 20\%$) (Figure 4). Further, this also leads to increase in the total number of mixed-orbitals as follows: **62** ($[\text{UO}_2.5\text{N}]^-$) $<$ **70** ($[\text{UO}_2.4\text{N1O}]$) $<$ **79** ($[\text{UO}_2.3\text{N2O}]^+$) $<$ **86** ($[\text{UO}_2.2\text{N3O}]^{2+}$). Thus, it indicates an enhanced orbital-mixing between U and O donors. To get further insight on the orbital-mixing and its intensity, we computed overlap integrals that accounts for the overlap of fragment orbital i and j at the basis of fragment MOs (S_{ij} , equation 2). In order to focus exclusively on the overlap at the equatorial plane, we have chosen UO_2^{2+} and L^n ($n=\text{charge of L}$) as fragments and computed the overlap-matrix using Multiwfn.⁶⁰

$$S_{ij} = \int \phi_i(r)\phi_j(r) d\tau \quad (2)$$

For the analysis with overlap-matrix, we screened the fragment molecular orbitals (FMOs)

based on the U($> 20\%$) and O_{eq}/N donor character, respectively. For FMOs with N character($> 20\%$), the resulted histograms shows sharp reduction in the frequency of S_{ij} upon decrease in number of N donors($> 20\%$) (Supporting information, left panel, Figure S3). Whereas, for FMOs with O_{eq} character, we noted an enhancement in the instances of overlaps between the fragments as we traverse from 4N1O to 3N2O to 2N3O, but with relatively low magnitude as compared to the case of N donor (Supporting information, right panel, Figure S3). This suggests that the replacement of N with O does not proportionately counter the decrease in overlap occurrences. Further, it can be noticed that the maximum value of S_{ij} is higher for N-donor based fragments as compared to O-donor-based fragments, supporting better overlap between FMOs with U and N character. Note that, as the considered FMOs are not pure metal or O_{eq}/N orbitals, the present analysis cannot provide exact information about the U-O/N overlap. Nevertheless, it effectively captures the changes in the degree of overlap upon donor substitution. These observations commensurate well with our findings of MO and DOS analysis.

3.3.3. Energy Decomposition Analysis (EDA) with ETS-NOCV:

We now focus on the energetic contribution associated with the donor-acceptor bonding. Here, we rely on EDA calculations using same fragment compositions (*i.e.* UO_2^{2+} and L^n) that we used in overlap-matrix generation. As mentioned earlier (see Computational section), EDA decompose the bonding strength of fragments (ΔE_{bond}) into various energy-components (ΔE_{ion} , ΔE_{orb} , ΔE_{Pauli}) (Table 4). Evidently, electrostatic interaction (ΔE_{ion}) acts as the major stabilizing component in the bonding energy. We noted that with increase in O donor at equatorial plane the repulsive ΔE_{Pauli} also increases, suggesting progressive destabilization due to the enhanced interaction between the electrons of UO_2^{2+} and ligand with same spin. The important role of ΔE_{Pauli} into the overall strength of interaction can be clearly understood by noting the trend in ΔE_{bond} . Interestingly, we noticed an increase in the percentage of ΔE_{orb} contribution (into ΔE_{bond}) from 5N to 2N3O. This can be rationalized with

our prior analysis of mixed molecular orbitals. The increase in the number of mixed-orbitals with more O donors allows larger orbital contribution.

Table 4: Contribution of interaction energy terms from EDA analysis of the complexes.^a

Complex	Pauli repulsion (ΔE_{Pauli})	Electrostatic Interaction (ΔE_{ion})	Orbital Interactions (ΔE_{orb})	Total bonding Energy (ΔE_{bond})
[UO ₂ .5N] ⁻	187.31 (-23.19 %)	-718.31 (88.96 %)	-276.41 (34.23 %)	-807.41
[UO ₂ .4N1O]	186.16 (-28.76 %)	-567.89 (87.75 %)	-265.40 (41.01 %)	-647.13
[UO ₂ .3N2O] ⁺	182.22 (-37.63 %)	-415.49 (85.81 %)	-250.90 (51.81 %)	-484.18
[UO ₂ .2N3O] ⁺²	170.90 (-53.23 %)	-255.18 (79.49 %)	-236.74 (73.74 %)	-321.02

All values are in kcal.mol⁻¹. ^aValues in parentheses correspond to the individual contributions of ΔE_{ion} , ΔE_{Pauli} , and ΔE_{orb} in the total bonding energy (ΔE_{bond}).

Another approach to understand the orbital energy contribution is to breakdown ΔE_{orb} into pairwise contribution of the relevant molecular orbitals (ΔE_k^{orb}) to characterize σ and π bonds between molecular fragments applying ETS-NOCV scheme.

$$\Delta E_{orb} = \sum_{k=1}^{N/2} \Delta E_k^{orb} \quad (3)$$

Several deformation density channels that contribute in the ΔE_{orb} values significantly are shown Figure 8. The flow of electron density occurs from red (depletion) to blue zone (accumulation). For all the complexes, first two dominant deformation density channels ($\Delta\rho_1$, $\Delta\rho_2$) indicate charge transfer from N donor to the metal center via σ donation, and contribute significantly with ΔE_k ranging from -27.3 to -47.9 kcal.mol⁻¹. The σ -donation from O atoms (of ring 1) are visible in the second deformation density channels of 4N1O, 3N2O and 2N3O. The contribution of other O atoms at the equatorial plane is found to be of weaker intensity. Interestingly, for uranyl complexes with 5N and 4N1O, $\Delta\rho_4$ and $\Delta\rho_5$ density channels shows π back-donation from metal center to the N, whereas no such instances are noted for rest of the complexes. The overall charge of these complexes can be a contributing factor behind this observation. The change in charge of the complexes makes U more positive (see NPA analysis) and subsequently less capable for back-donation as one approach from 5N to 4N1O to 3N2O to 2N3O.

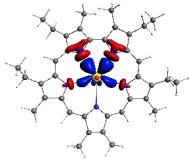
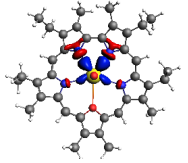
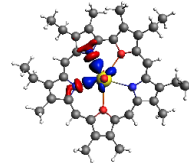
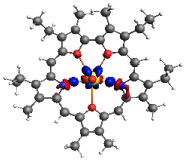
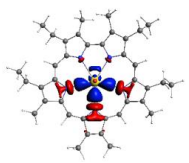
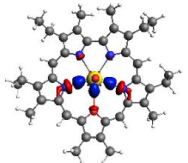
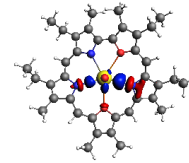
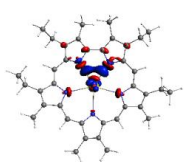
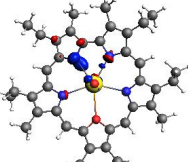
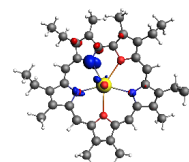
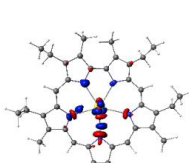
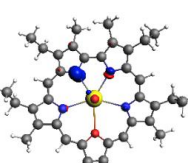
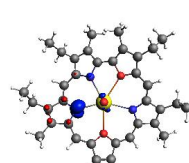
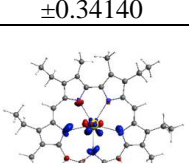
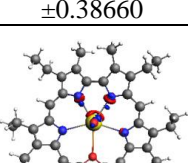
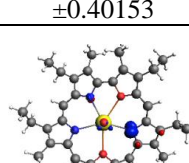
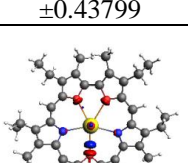
Deformation Channel	$[\text{UO}_2.5\text{N}]^-$	$[\text{UO}_2.4\text{N}1\text{O}]$	$[\text{UO}_2.3\text{N}2\text{O}]^+$	$[\text{UO}_2.2\text{N}3\text{O}]^{+2}$
1				
ΔE_{k1}	-41.7	-47.9	-42.8	-27.3
Eigenvalue	± 0.57241	± 0.59846	± 0.57174	± 0.54301
2				
ΔE_{k2}	-42.7	-35.0	-35.2	-42.1
Eigenvalue	± 0.52658	± 0.48868	± 0.47317	± 0.49478
3				
ΔE_{k3}	-23.3	-22.0	-21.1	-21.8
Eigenvalue	± 0.36503	± 0.39155	± 0.41390	± 0.44566
4				
ΔE_{k4}	-18.2	-19.6	-19.4	-23.0
Eigenvalue	± 0.34140	± 0.38660	± 0.40153	± 0.43799
5				
ΔE_{k5}	-14.7	-18.3	-15.5	-17.5
Eigenvalue	± 0.33177	± 0.33602	± 0.33848	± 0.28013

Figure 8: Important deformation density channels with eigenvalues of the complexes from ETS-NOCV analysis. (isovalue: 0.003 au). All energy values are in kcal.mol^{-1}

3.3.4. QTAIM analysis

Though, it is evident from the charge and MO analysis that U-N bond has more covalent character as compared to U-O_{eq} bond, the interpretation about the nature of such covalency is somewhat difficult solely on these analyses. Based on the perturbation theory, the interaction between metal and ligand orbital may lead to two-types of covalency, namely overlap-driven and near-degeneracy driven covalency. The dominance of one over another is determined by following equation:

$$\lambda = \frac{H_{ij}}{E_i^0 - E_j^0} \quad (4)$$

Where, λ is the first-order mixing coefficient, H_{ij} is the off-diagonal Hamiltonian matrix element, and E_i^0 , E_j^0 are the energy of the fragment orbitals. Under the assumption of Wolfsberg–Helmholz approximation, H_{ij} is considered proportional to the overlap integral S_{ij} . Evidently, high λ can be achieved either by better overlap of orbitals (i.e. high S_{ij}) or through the lower energy gap between the fragment orbitals. The former case leads to overlap-driven covalency while the later results in near-degeneracy driven covalency accompanying delocalization of electronic states with minimum overlap.

The analysis on the S_{ij} at the preceding section throws some light into it as it suggested the dominance of orbital interactions with significantly low overlaps (between FMOs) for both the donors. The extent of the orbital overlap can be understood by quantifying the charge build-up at the middle of the bond.⁵³ In this regard, density-based QTAIM analysis has worked as consistent tool.^{21,48,50–52,61} Significantly small values of $\rho(r)$ ($\ll 0.2$ e/Bohr³) and positive $\nabla^2\rho$ for all the metal-ligand bonds at the equatorial plane indicate their predominant ionic character (Supporting information, Table S2). This complements the results of EDA and also supports the higher population of low overlap integrals (Supporting information, Figure S3). Though MO analysis indicates higher orbital-mixing in case of O donor, the distribution of overlap integral indicates their low amplitude. QTAIM confirms that

this has diminishing effect on the overall charge density. As a result, BCPs of U-N bonds have higher $\rho(r)$ than U-O_{eq}. The trend in H(r) further substantiate the higher covalent character for the former, and in accordance to the $\rho(r)$, such covalency carries signature of near-degeneracy driven covalency. In agreement with the optimized parameter, QTAIM descriptors also resolve the differential characters between N_{1,3,4} and N_{2,5}, and suggest higher covalent character for the U-N_{1,3,4} than U-N_{2,5}. Further analysis of bonded radii, R_b (*i.e.* distance between the BCP and donor center) indeed confirms that the former has significantly smaller R_b(N) than later (Supporting information, Figure S4). The ellipticity(ϵ) data supports bond order analysis (WBIs and DIs, Table 3), suggesting much lower ϵ for the U-O_{ax} bond as compared to the equatorial bond paths due to the cylindrically symmetrical nature of former bond. This is possibly due to the presence of two π bonds in two perpendicular planes along the bond axis resulting in formation of triple bond. Higher ϵ of the equatorial bonds indicates highly asymmetric electron density along the bond path.

It is evident from all these analyses that U prefers to bind with N than O atom. In this context, analysis of the trend in R_b data led to an interesting viewpoint on how N and O donors compete to interact with U in the mixed-donor environment (Supporting information, Figure S4). We believe that in case of 4N1O, the presence of four N donor centers efficiently compete with O₁ for metal bonding to induce high R_b (O₁) value, whereas successive decrease in the number of N donor centers in 3N2O to 2N3O helps in enhancing the interaction with O donor and thereby reduces the associated R_b (O) values. This finding also correlates with the increasing trend in $\rho(r)$ values of U-O bond as we traverse from 4N1O to 3N2O to 2N3O. Nevertheless, such substitutions with O donor also compel U to strengthen the existing U-N interaction, which is visible with the simultaneous increase in $\rho(r)$ values of U-N and U-O_{eq} values and decrease in associated bond-lengths with the increase in O donor atoms at cavity. In fact, trend in the average S_{ij} values per N atom follows the following order: 0.0029 (5N) < 0.0044 (4N1O) < 0.0065 (3N2O) < 0.0090 (2N3O), and indicates that reduction of N donor prompts better overlap between UO₂⁺ and remaining N atoms. Therefore, such competitive

aspect could also act as an additional driving force behind the subtle change in bonding characteristics of donor centers.

3.3.5. Thermodynamic stability of the complexes

Table 5: Thermodynamic data for complexes calculated using B3LYP functional.^a

System	Reorganisation Energy of ligand	ΔG	ΔS	ΔH
$[\text{UO}_2.5\text{N}]^-$	23.0	-107.66	-0.02	-114.19
$[\text{UO}_2.4\text{N1O}]$	9.3	-75.88	-0.02	-81.11
$[\text{UO}_2.3\text{N2O}]^+$	8.2	-41.11	-0.01	-45.43
$[\text{UO}_2.2\text{N3O}]^{2+}$	8.9	-3.25	-0.01	-6.85

^aall free energy values are in kcal.mol⁻¹. ΔS values are in kcal.mol⁻¹.K⁻¹ unit

Finally, we draw our attention to the translation of the electronic structure calculations into the thermodynamic stability of the complexes through the analysis of binding free energies (ΔG_{bind}) (Table 5 and Supporting information, Table S3). We found that the successive substitution of N with O donor led to decrease in ΔG_{bind} values with $[\text{UO}_2.5\text{N}]^-$ as the most thermodynamically favorable complex. This is in good agreement with the trend in EDA-based ΔE_{bond} and with the LMCT. Therefore, the electrostatic interaction and associated charge-transfer act here as the deciding factor, which is not so surprising in the context of charge variation of the ligands. Further, more covalent character of U-N bonds as compared to U-O bonds helps gaining additional stability with higher population of N donors at the cavity. Arguably, another aspect that might contribute to the overall stabilization of the complex is *via* aromaticity. The idea of such chelatoaromatic stabilization has been pitched⁶² back in 1945, and recent studies^{19,21,48} suggested it as an important contributing factor on actinide complexation. Here, we touch upon this aspect by analyzing the geometric Harmonic oscillator model of aromaticity index (HOMA), which can be applied advantageously on fragments as well as on the whole complex.⁶³ The extent of aromatic character is determined

by the magnitude and sign of HOMA value. Positive value indicate the aromatic character, while negative HOMA value suggest antiaromaticity. It is evident from the calculated HOMA values of furan and pyrrole rings of ligands (with and without complexation) that uranyl offers chelato-aromatic stabilization by enhancing aromatic character of the ligand (Supporting information, Table S4). However, such stabilization is solely associated with pyrrole rings as with increasing N donor substitution with O enhances the anti-aromatic character within the ligand. Therefore, it corroborates well with the obtained trend of binding free energy. Apparently, the chelatoaromatic stabilization can be broadly considered as the consequence of underlying electronic effects within the complex, that has been studied in-depth in this work. Here, it is important to mention that unlike $[\text{UO}_2.4\text{N1O}]$ complex where experimental report on complexation is available,²⁶ however, synthesis of $[\text{UO}_2.5\text{N}]^-$ led to many unsuccessful attempts and resulted into a dearomatized product with ‘-OMe’ substitution in the presence of methanol.⁶⁴ This is somewhat counter-intuitive to our predicted free-energy trend. Previous DFT investigation led by Shamov pointed possible few reasons behind this including the highly basic nature of trianionic sapphyrin ligand (5N).⁶⁵ Undoubtedly, the simple reaction scheme used here is unable to capture the intrinsic mechanism behind the complex formation. The detailed investigation on this aspect is beyond the scope of present study. Nevertheless, the trend in reorganization energies (of ligands) suggests significantly higher positive value ($+23 \text{ kcal.mol}^{-1}$) for 5N as compared to other ligands ($+9 \text{ kcal.mol}^{-1}$), which also can be a contributing factor behind the experimental difficulty on $[\text{UO}_2.5\text{N}]^-$ synthesis (Table 5).

4. Conclusion

The quest for macrocyclic ligands to efficiently sequester U(VI) has been on for decades. Important structural attributes of the ligands such as the characteristics of donor-centers (hard or soft) and their number at the cavity are known to controls the efficiency of the

ligands by providing the essential bonding scenario for uranyl. Further, the composition of donor-centers at ligand core becomes particularly important in case of mixed-donor ligand environment. In this present study, with the aid of orbital and density-based analyses, we scrupulously investigated how and at what extent change in the type and number of N and O donors at the cavity of expanded-porphyrin impact the bonding characteristics of uranyl. Our in-depth MO and DOS analyses show strong and favorable participation of U(d) into bonding with donor's p orbitals, U(f)-orbitals participate in much lower extent. Whereas, the interaction of donors with U(p) shows antibonding characteristics. Our results confirm that in the expanded porphyrins, UO_2^{2+} has preference for N over O donor. Deformation density channels obtained from the ETS-NOCV analysis show that N and O both act as σ donor to uranyl but the intensity of such donation is higher for former. The π back-donation from uranyl to ligand is noted only for 5N and 4N1O systems, but the deficiency in charge transfer restricts the capability of such back-donation for 3N2O and 2N3O. EDA, NPA along with thermodynamic analyses confirms the dominance of electrostatic interaction on the thermodynamic stability of the complexes. However, the U-N/O bonds at the equatorial plane do carry appreciable covalent character, but analysis of QTAIM descriptors in conjugation with MO analysis and overlap integral calculations confirms its nature as near-degeneracy driven type. Based on statistics of mixed-orbitals and overlap integrals, we further demonstrated that the O donor does not act as adequate or efficient replacement for uranyl binding. Though, MO analysis indicated that the presence of O donors increases orbital mixing by forming more mixed-orbitals with uranyl but the amplitude of overlap among FMOs does not match with the N donors. It is anticipated that the findings presented in the present study will not only help understanding the role of O substitution in expanded porphyrin but also assist on setting design criteria for actinide chelation in macrocyclic environment.

References

- (1) Macfarlane, A. M.; Miller, M. Nuclear energy and uranium resources. *Elements* **2007**, *3*, 185–192.
- (2) Natrajan, L. S. Developments in the photophysics and photochemistry of actinide ions and their coordination compounds. *Coordination Chemistry Reviews* **2012**, *256*, 1583–1603.
- (3) Wang, S.; Alekseev, E. V.; Diwu, J.; Miller, H. M.; Oliver, A. G.; Liu, G.; Depmeier, W.; Albrecht-Schmitt, T. E. Functionalization of borate networks by the incorporation of fluoride: syntheses, crystal structures, and nonlinear optical properties of novel actinide fluoroborates. *Chemistry of Materials* **2011**, *23*, 2931–2939.
- (4) Degueudre, C. A.; Dawson, R. J.; Najdanovic-Visak, V. Nuclear fuel cycle, with a liquid ore and fuel: toward renewable energy. *Sustainable Energy & Fuels* **2019**, *3*, 1693–1700.
- (5) Tsouris, C. Uranium extraction: fuel from seawater. *Nature Energy* **2017**, *2*, 1–3.
- (6) Sun, Q.; Aguila, B.; Perman, J.; Ivanov, A. S.; Bryantsev, V. S.; Earl, L. D.; Abney, C. W.; Wojtas, L.; Ma, S. Bio-inspired nano-traps for uranium extraction from seawater and recovery from nuclear waste. *Nature communications* **2018**, *9*, 1–9.
- (7) Lu, Y. Uranium extraction: coordination chemistry in the ocean. *Nature chemistry* **2014**, *6*, 175.
- (8) Aguila, B.; Sun, Q.; Cassady, H.; Abney, C. W.; Li, B.; Ma, S. Design strategies to enhance amidoxime chelators for uranium recovery. *ACS applied materials & interfaces* **2019**, *11*, 30919–30926.
- (9) Madic, C.; Hudson, M. J. High-Level Liquid Waste Partitioning by Means of Completely Incinerable Extractants. *EUR 18038 EN, European Commission, Luxembourg* **1998**,

- (10) Rogers, R. D.; Bond, A. H.; Hipple, W. G.; Rollins, A. N.; Henry, R. F. Synthesis and structural elucidation of novel uranyl-crown ether compounds isolated from nitric, hydrochloric, sulfuric, and acetic acids. *Inorganic chemistry* **1991**, *30*, 2671–2679.
- (11) Gong, Y.; Gibson, J. K. Crown ether complexes of uranyl, neptunyl, and plutonyl: Hydration differentiates inclusion versus outer coordination. *Inorganic chemistry* **2014**, *53*, 5839–5844.
- (12) Leydier, A.; Lecercle, D.; Pellet-Rostaing, S.; Favre-Reguillon, A.; Taran, F.; Lemaire, M. Sequestering agents for uranyl chelation: new calixarene ligands. *Tetrahedron* **2008**, *64*, 11319–11324.
- (13) Thuéry, P.; Masci, B. Uranyl ion complexation by cucurbiturils in the presence of perhenic, phosphoric, or polycarboxylic acids. Novel mixed-ligand uranyl-organic frameworks. *Crystal growth & design* **2010**, *10*, 716–725.
- (14) Brewster, J. T.; Zafar, H.; Root, H. D.; Thiabaud, G. D.; Sessler, J. L. Porphyrinoid f-element complexes. *Inorganic chemistry* **2019**, *59*, 32–47.
- (15) Brewster, J. T.; Mangel, D. N.; Gaunt, A. J.; Saunders, D. P.; Zafar, H.; Lynch, V. M.; Boreen, M. A.; Garner, M. E.; Goodwin, C. A.; Settineri, N. S., et al. In-plane thorium (IV), uranium (IV), and neptunium (IV) expanded porphyrin complexes. *Journal of the American Chemical Society* **2019**, *141*, 17867–17874.
- (16) Brewster, J. T.; Root, H. D.; Mangel, D.; Samia, A.; Zafar, H.; Sedgwick, A. C.; Lynch, V. M.; Sessler, J. L. UO_2^{2+} -mediated ring contraction of pyrihexaphyrin: synthesis of a contracted expanded porphyrin-uranyl complex. *Chemical science* **2019**, *10*, 5596–5602.
- (17) Herasymchuk, K.; Chiang, L.; Hayes, C. E.; Brown, M. L.; Ovens, J. S.; Patrick, B. O.; Leznoff, D. B.; Storr, T. Synthesis and electronic structure determination of uranium (VI) ligand radical complexes. *Dalton Transactions* **2016**, *45*, 12576–12586.

- (18) Mayhugh, J. T.; Niklas, J. E.; Forbes, M. G.; Gorden, J. D.; Gorden, A. E. Pyrrophenes: Pyrrole-Based Hexadentate Ligands Tailor-Made for Uranyl (UO_2^{2+}) Coordination and Molecular Recognition. *Inorganic Chemistry* **2020**, *59*, 9560–9568.
- (19) Ho, I.-T.; Zhang, Z.; Ishida, M.; Lynch, V. M.; Cha, W.-Y.; Sung, Y. M.; Kim, D.; Sessler, J. L. A hybrid macrocycle with a pyridine subunit displays aromatic character upon uranyl cation complexation. *Journal of the American Chemical Society* **2014**, *136*, 4281–4286.
- (20) Yang, Y.; Zhang, Z.; Yang, L.; Liu, J.; Xu, C.; Luo, S.; Rao, L. Complexation of U(VI) with BiPDA, DmBiPDA, and PhenDA: comparison on structures and binding strengths in aqueous and DMSO/20%(v) H₂O solutions. *Inorganic chemistry* **2019**, *58*, 6064–6074.
- (21) Sadhu, B.; Dolg, M. Enhancing actinide (III) over lanthanide (III) selectivity through hard-by-soft donor substitution: exploitation and implication of near-degeneracy-driven covalency. *Inorganic chemistry* **2019**, *58*, 9738–9748.
- (22) Varathan, E.; Gao, Y.; Schreckenbach, G. Computational Study of Actinyl Ion Complexation with Dipyrimethyrin Macrocylic Ligands. *The Journal of Physical Chemistry A* **2021**, *125*, 920–932.
- (23) Sadhu, B.; Sundararajan, M.; Bandyopadhyay, T. Efficient separation of europium over americium using cucurbit-[5]-uril supramolecule: a relativistic DFT based investigation. *Inorganic chemistry* **2016**, *55*, 598–609.
- (24) Di Pietro, P.; Kerridge, A. Ligand size dependence of U–N and U–O bond character in a series of uranyl hexaphyrin complexes: quantum chemical simulation and density based analysis. *Physical Chemistry Chemical Physics* **2017**, *19*, 7546–7559.
- (25) Hu, S.-X.; Li, W.-L.; Dong, L.; Gibson, J. K.; Li, J. Crown ether complexes of actinyls:

- a computational assessment of AnO₂ (15-crown-5) 2+(An= U, Np, Pu, Am, Cm). *Dalton Transactions* **2017**, *46*, 12354–12363.
- (26) Sessler, J. L.; Gebauer, A.; Hoehner, M. C.; Lynch, V. Synthesis and characterization of an oxasapphyrin-uranyl complex. *Chemical Communications* **1998**, 1835–1836.
- (27) Broadhurst, M.; Grigg, R.; Johnson, A. New macrocyclic aromatic systems related to porphins. *Journal of the Chemical Society D: Chemical Communications* **1969**, 23–24.
- (28) Becke, A. D. Density-functional exchange-energy approximation with correct asymptotic behavior. *Physical review A* **1988**, *38*, 3098.
- (29) Perdew, J. P. Density-functional approximation for the correlation energy of the inhomogeneous electron gas. *Physical Review B* **1986**, *33*, 8822.
- (30) Weigend, F.; Ahlrichs, R. Balanced basis sets of split valence, triple zeta valence and quadruple zeta valence quality for H to Rn: Design and assessment of accuracy. *Physical Chemistry Chemical Physics* **2005**, *7*, 3297–3305.
- (31) Schäfer, A.; Huber, C.; Ahlrichs, R. Fully optimized contracted Gaussian basis sets of triple zeta valence quality for atoms Li to Kr. *The Journal of Chemical Physics* **1994**, *100*, 5829–5835.
- (32) Dolg, M.; Stoll, H.; Preuss, H. Energy-adjusted abinitio pseudopotentials for the rare earth elements. *The Journal of chemical physics* **1989**, *90*, 1730–1734.
- (33) Küchle, W.; Dolg, M.; Stoll, H.; Preuss, H. Energy-adjusted pseudopotentials for the actinides. Parameter sets and test calculations for thorium and thorium monoxide. *The Journal of chemical physics* **1994**, *100*, 7535–7542.
- (34) a development of University of Karlsruhe and Forschungszentrum Karlsruhe GmbH, 1989–2007, TURBOMOLE GmbH, since 2007, available from <http://www.turbomole.com>. *TURBOMOLE V7.2* **2017**,

- (35) Becke, A. D. Density-functional thermochemistry. III. The role of exact exchange. *J. Chem. Phys* **1993**, *98*, 5648–6.
- (36) Lee, C.; Yang, W.; Parr, R. G. Development of the Colle-Salvetti correlation-energy formula into a functional of the electron density. *Physical review B* **1988**, *37*, 785.
- (37) Lenthe, E. v.; Baerends, E.-J.; Snijders, J. G. Relativistic regular two-component Hamiltonians. *The Journal of chemical physics* **1993**, *99*, 4597–4610.
- (38) Neese, F.; Wennmohs, F. ORCA (v. 3.0. 3). *An ab initio, DFT and semiempirical SCF-MO package, Max-Planck-Institute for Chemical Energy Conversion, Stifstr* **2013**, 34–36.
- (39) Neese, F.; Wennmohs, F.; Hansen, A.; Becker, U. Efficient, approximate and parallel Hartree–Fock and hybrid DFT calculations. A ‘chain-of-spheres’ algorithm for the Hartree–Fock exchange. *Chemical Physics* **2009**, *356*, 98–109.
- (40) Takano, Y.; Houk, K. Benchmarking the conductor-like polarizable continuum model (CPCM) for aqueous solvation free energies of neutral and ionic organic molecules. *Journal of Chemical Theory and Computation* **2005**, *1*, 70–77.
- (41) Atta-Fynn, R.; Johnson, D. F.; Bylaska, E. J.; Ilton, E. S.; Schenter, G. K.; De Jong, W. A. Structure and hydrolysis of the U (IV), U (V), and U (VI) aqua ions from ab initio molecular simulations. *Inorganic chemistry* **2012**, *51*, 3016–3024.
- (42) Spencer, S.; Gagliardi, L.; Handy, N. C.; Ioannou, A. G.; Skylaris, C.-K.; Willetts, A.; Simper, A. M. Hydration of UO_2^{2+} and PuO_2^{2+} . *The Journal of Physical Chemistry A* **1999**, *103*, 1831–1837.
- (43) Grimme, S. Semiempirical hybrid density functional with perturbative second-order correlation. *The Journal of chemical physics* **2006**, *124*, 034108.

- (44) Kitaura, K.; Morokuma, K. A new energy decomposition scheme for molecular interactions within the Hartree-Fock approximation. *International Journal of Quantum Chemistry* **1976**, *10*, 325–340.
- (45) Van Lenthe, E.; Baerends, E. J. Optimized Slater-type basis sets for the elements 1–118. *Journal of computational chemistry* **2003**, *24*, 1142–1156.
- (46) Te Velde, G. t.; Bickelhaupt, F. M.; Baerends, E. J.; Fonseca Guerra, C.; van Gisbergen, S. J.; Snijders, J. G.; Ziegler, T. Chemistry with ADF. *Journal of Computational Chemistry* **2001**, *22*, 931–967.
- (47) Mitoraj, M. P.; Michalak, A.; Ziegler, T. On the nature of the agostic bond between metal centers and β -hydrogen atoms in alkyl complexes. An analysis based on the extended transition state method and the natural orbitals for chemical valence scheme (ETS-NOCV). *Organometallics* **2009**, *28*, 3727–3733.
- (48) Sadhu, B.; Mishra, V. The coordination chemistry of lanthanide and actinide metal ions with hydroxypyridinone-based decorporation agents: orbital and density based analyses. *Dalton Transactions* **2018**, *47*, 16603–16615.
- (49) Clark, A. E.; Sonnenberg, J. L.; Hay, P. J.; Martin, R. L. Density and wave function analysis of actinide complexes: What can fuzzy atom, atoms-in-molecules, Mulliken, Löwdin, and natural population analysis tell us? *The Journal of chemical physics* **2004**, *121*, 2563–2570.
- (50) Kaltsoyannis, N. Does covalency increase or decrease across the actinide series? Implications for minor actinide partitioning. *Inorganic chemistry* **2013**, *52*, 3407–3413.
- (51) Kerridge, A. Quantification of f-element covalency through analysis of the electron density: insights from simulation. *Chemical Communications* **2017**, *53*, 6685–6695.

- (52) Su, J.; Batista, E. R.; Boland, K. S.; Bone, S. E.; Bradley, J. A.; Cary, S. K.; Clark, D. L.; Conradson, S. D.; Ditter, A. S.; Kaltsoyannis, N., et al. Energy-degeneracy-driven covalency in actinide bonding. *Journal of the American Chemical Society* **2018**, *140*, 17977–17984.
- (53) Neidig, M. L.; Clark, D. L.; Martin, R. L. Covalency in f-element complexes. *Coordination Chemistry Reviews* **2013**, *257*, 394–406.
- (54) Bader, R. F. A quantum theory of molecular structure and its applications. *Chemical Reviews* **1991**, *91*, 893–928.
- (55) Bader, R.; Bader, R. *Atoms in Molecules: A Quantum Theory*; International series of monographs on chemistry; Clarendon Press, 1990.
- (56) Bader, R. F. Atoms in molecules. *Accounts of Chemical Research* **1985**, *18*, 9–15.
- (57) Sessler, J. L.; Weghorn, S. J.; Weghorn, S. J. *Expanded, contracted & isomeric porphyrins*; Elsevier, 1997; Vol. 15.
- (58) Broadhurst, M.; Grigg, R.; Johnson, A. The synthesis of 22 π -electron macrocycles. Sapphyrins and related compounds. *Journal of the Chemical Society, Perkin Transactions 1* **1972**, 2111–2116.
- (59) Outeiral, C.; Vincent, M. A.; Pendás, Á. M.; Popelier, P. L. Revitalizing the concept of bond order through delocalization measures in real space. *Chemical science* **2018**, *9*, 5517–5529.
- (60) Lu, T.; Chen, F. Multiwfn: a multifunctional wavefunction analyzer. *Journal of computational chemistry* **2012**, *33*, 580–592.
- (61) Sadhu, B.; Dolg, M.; Kulkarni, M. S. Periodic trends and complexation chemistry of tetravalent actinide ions with a potential actinide decorporation agent 5-LIO (Me-3, 2-

- HOPO): A relativistic density functional theory exploration. *Journal of computational chemistry* **2020**, *41*, 1427–1435.
- (62) Calvin, M.; Wilson, K. Stability of chelate compounds. *Journal of the American Chemical Society* **1945**, *67*, 2003–2007.
- (63) Krygowski, T. M. Crystallographic studies of inter-and intramolecular interactions reflected in aromatic character of pi.-electron systems. *Journal of chemical information and computer sciences* **1993**, *33*, 70–78.
- (64) Burrell, A. K.; Cyr, M. J.; Lynch, V.; Sessler, J. L. Nucleophilic attack at the meso position of a uranyl sapphyrin complex. *Journal of the Chemical Society, Chemical Communications* **1991**, 1710–1713.
- (65) Shamov, G. A. Oxidative nucleophilic substitution of hydrogen in the sapphyrin dioxouranium (VI) complex: a relativistic DFT study. *Journal of the American Chemical Society* **2011**, *133*, 4316–4329.

Acknowledgement

SC and BS thank Dr. M. S. Kulkarni, Head, HPD for his continuous support and encouragement. Authors thank Dr. Ashokkumar P., Shri R. V. Kolekar, Dr. R. K. Gopalakrishnan, Dr. P. K. Mohapatra (Head, Actinide Chemistry Section) and Dr. P. K. Pujari (Head, RCD and Director, RC & IG). Authors also grateful to ANUPAM Supercomputing Facility, Bhabha Atomic Research Center, India for the computational resources.

Supporting Information Available

MO energy diagram (Distribution of U(s)- and U(p)-based orbitals), MO energy diagram (Distribution of donor center orbitals for bare ligands), results on overlap integrals, QTAIM

analysis, plot on bonded radii, Thermodynamic data for all density functionals, aromaticity analysis.

Graphical TOC Entry

